POLYPUBLIE
Polytechnique Montréal

POLYTECHNIQUE MONTRÉAL
UNIVERSITÉ D'INGÉNIERIE

Document en libre accès dans PolyPublie
Open Access document in PolyPublie

Document publié chez l'éditeur officiel
Document issued by the official publisher

Erratum

A calibration error on our radiometer led us to misreport irradiance values for the UVC lamps used in our original manuscript.

The original statement:

> *The precursor gas mixture (H_2 and CO) was injected in the reactor with a molar ratio of 0.1/1 (H_2/CO) and was irradiated by two UVC lamps (main emission peak at 253.7 nm, irradiance of 5.5×10^{-4} W/cm^2 at 4.5 cm).*

The corrected statement:

> *The precursor gas mixture (H_2 and CO) was injected in the reactor with a molar ratio of 0.1/1 (H_2/CO) and was irradiated by two UVC lamps (main emission peak at 253.7 nm, irradiance of* 0.01 W/cm^2 at 3.5 cm*).*

Charge Effect of Superparamagnetic Iron Oxide Nanoparticles on their Surface Functionalization by Photo-Initiated Chemical Vapor Deposition

Taraneh Javanbakht[1], Sophie Laurent[2,3], Dimitri Stanicki[2], Wendell Raphael[1], Jason Robert Tavares[1*]

[1]Department of Chemical Engineering, Ecole Polytechnique of Montreal, Montreal, Quebec, Canada H3C 3A7

[2]Laboratory of NMR and Molecular Imaging, University of Mons, Avenue Maistriau 19, B-7000 Mons, Belgium

[3]Center for Microscopy and Molecular Imaging (CMMI), 6041 Gosselies, Belgium

*Corresponding author: Jason Robert Tavares

email: jason.tavares@polymtl.ca

telephone: +1 (514) 340-4711, x2326

Key words: superparamagnetic iron oxide nanoparticles, PICVD, contact angle, FTIR, TEM, XPS

Abstract

Diverse applications of superparamagnetic iron oxide nanoparticles (SPIONs) in the chemical and biomedical industry depend on their surface properties. In this paper, we investigate the effect of initial surface charge (bare, positively and negatively charged SPIONs) on the resulting physicochemical properties of the particles following treatment through photo-initiated chemical vapour deposition (PICVD). Transmission electron microscopy shows a nanometric polymer coating on the SPIONs and contact angle measurements with water demonstrate that their surface became non-polar following functionalization using PICVD. FTIR and XPS data confirm the change in the chemical composition of the treated SPIONs. Indeed, XPS data reveal an initial charge-dependent increase in the surface oxygen content in the case of treated SPIONs. The O/C percentage ratios of the bare SPIONs increase from 1.7 to 1.9 after PICVD treatment, and decrease from 1.7 to 0.7 in the case of negatively-charged SPIONs. The ratio remains unchanged for positively-charged SPIONs (1.7). This indicates that bare and negatively charged SPIONs showed opposite preference for the oxygen or carbon attachment to their surface during their surface treatment. These results reveal that both the surface charge and stereochemical effects have determinant roles in the polymeric coating of SPIONs with PICVD. Our findings suggest that this technique is appropriate for the treatment of nanoparticles.

Introduction

The applications of superparamagnetic iron oxide nanoparticles (SPIONs) in various fields have been improved considerably in recent years. Among many applications, superparamagnetic nanosystems can be used for magnetic data storage (Eigler et al. 2014), polluting agent removal (Nethaji et al. 2013), or, more recently as catalysts for organic reactions (Gawande et al. 2013, Obermayer et al. 2013). Beside these numerous applications, SPIONs are widely used nanomaterials for biomedical purposes, such as magnetic resonance imaging (MRI) (Chen et al. 2011), hyperthermia for cancer therapy (Jin et al. 2008), cell targeting (Das et al. 2008), drugs or gene delivery (Namvari and Namazi 2014). Their interaction within the body once introduced into the blood stream depends on their surface properties. These nanoparticles (NPs) can be captured by the macrophages and then rapidly cleared out from circulation, which can drastically reduce their efficiency in the body (Fan et al. 2011). Therefore, their surface functionalization and the investigation of their physicochemical properties are very important for their diverse applications. SPIONs can be synthesized by diverse methods such as co-precipitation (Uzun et al. 2010), thermal decomposition (Sun and Zeng 2002), microemulsion (Solans et al. 2005), hydrothermal synthesis (Hu et al. 2007) and sonochemistry (Vijayakumar et al. 2000). A suitable surface functionalization and choice of solvent are crucial in order to obtain sufficient repulsive interactions to prevent agglomeration of SPIONs. In the absence of any proper surface coating, the interactions between these nanoparticles will cause them to aggregate and form large clusters (Chang et al. 2007). It is also needed to enhance their biocompatibility in *in vitro* and *in vivo* studies (Hanini et al. 2011). For example, liposomes and micelles, spherical aggregates of amphiphilic molecules, can be used to coat SPIONs (Veiseh et al. 2010). In other words, functionalization to improve colloidal stability is necessary for end-use applications and long-term storage.

Surface functionalization of nanomaterials includes simple or complex physical or chemical procedures that involve weak electrostatic repulsion, hydrogen bonding, hydrophobic interactions or covalent bonds, respectively (Wang et al. 2009). One study showed that coating SPIONs with a gold layer enabled subsequent functionalization with thiolated DNA, which could then remain stable in aqueous solution (Robinson et al. 2010). PEG-siloxane ligands have been shown to promote the colloidal stability of SPIONs (Bloemen et al. 2014; Chen et al. 2009), though the authors have not

reported any surface characterization of the coated nanoparticles. The use of organic solvents in these studies may change the surface composition of SPIONs and sometimes cause the addition of some chemical elements on their surface, meaning!the presence of contaminants on their surface, which was not indicated.

Surfactants, such as sulphuric lycine, may also be employed (Wu et al. 2008). However, none of these reports related the effect of initial surface charge and composition of SPIONs (resulting from the synthesis approach) on functionalization (Neouze and Schubert 2008; Latham and Williams 2008; De Palma et al. 2007; Matsuno et al. 2004; Georgelin et al. 2008). This is significant because surface charge and composition can impact the electrostatic interaction of the SPIONs with the polymer coating.

Previously, our group designed and developed a new, solvent-free and scalable surface functionalization technique called photo-initiated chemical vapor deposition (PICVD) (Dion et al. 2014). In this work, we carry out surface functionalization of SPIONs using PICVD, and assess its impact as a secondary functionalization tool on the physicochemical properties of these nanomaterials as a function of their initial surface charge.

Materials and methods

Chemicals. Sodium hydroxide (5 M), hydrogen peroxide (50%), acetone (ACS reagent, $\geq99.0\%$), diethylic ether (ACS reagent, $\geq99.0\%$), dimethylformamide anhydrous HPLC, n-[3-(trimethoxysilyl)propyl] ethylenediamine (TPED) (97%) were purchased at Sigma-Aldrich. HPLC-grade methanol was purchased at ChemLab. Diethylene glycol (> 99%), iron (II) chloride tetrahydrate (99%) were purchased at Merck and iron (III) chloride solution (45%) was purchased at Riedel-de Ha'n.1-ethyl-3-(3-dimethylaminopropyl) carbodiimide (>98%), and tetramethylammonium hydroxide (>95%) were purchased at TCI Chemicals, while 3-(triethoxysilyl)propyl succinic anhydride (TEPSA) (>94%) was purchased at ABCR.

Nanoparticle preparation. Bare SPIONs: 5 ml of an aqueous solution of $FeCl_2.4H_2O$ (0.045 M) and $FeCl_3.6H_2O$ (0.0375 M) were added to 250 ml of diethylene glycol. The mixture was heated to 170 ¡C and maintained at this temperature for 15 min before addition of the base (i.e. solid NaOH until a final concentration of 0.375 M). Subsequently, temperature was maintained at 170 ¡C for a period of 1 h before cooling to 60 ¡C. The synthesized SPIONs were collected with a neodymium magnet and washed with 100 ml of a HNO_3 (1 M) solution.

Negatively charged SPIONs (with carboxylate functions) (Stanicki et al. 2014): 14.2 ml of 3-(triethoxysilyl)propylsuccinic anhydride (TEPSA, 50 mmol) were slowly added to a nanoparticle suspension in DMF (100 mM of iron in 100 ml). 8.6 ml of water followed by 5 ml of TMAOH solution (1 M) were added at room temperature and under homogenization. The solution was heated to 100 ¡C for 24 h under continuous stirring. The SPIONs were precipitated by addition of acetone/ether (50/50) mixture and collected with a neodymium magnet. The precipitate was washed with acetone several times and finally dispersed in water. Excess of silane derivative and other chemicals were removed by membrane filtration (cut-off of the membrane is 30,000 Da).

Positively charged SPIONs (with amino functions): N-[3-(trimethoxysilyl)propyl] ethylenediamine (TPED) was grafted onto SPIONs by adding 25 mmol of TPED (5.4 ml) to a suspension of NP (100 ml, [Fe] = 25 mM) at 50¡C. After stirring for 2h at reflux, the mixture was cooled at room temperature and the suspension was purified by membrane filtration (membrane cut-off: 30 kDa), and then centrifuged (16,500 g; 45 minutes).

Photo-initiated chemical vapor deposition. The surface modification of the SPIONs was carried out in a PICVD micro-reactor illustrated in Figure 1 and detailed extensively in (Dion et al. 2014). 50 µL of the SPIONs suspension were deposited onto polished copper sample holders three successive times and allowed to dry at room temperature for 24 hours. The copper sample holders were polished beforehand using deionized water and sandpaper (grit 1200 MX); Cu was retained as a sample holder for it was the material used in the initial PICVD investigation (Dion et al. 2014). The SPIONs to be treated were placed inside the tubular quartz reactor at a distance of 40 cm from the inlet. Before each treatment sequence, argon was used to purge the reactor for 3 minutes. The precursor gas mixture (H_2 and CO) was injected in the reactor with a molar ratio of 0.1/1 (H_2/CO) and was irradiated by two UVC

lamps (main emission peak at 253.7 nm, irradiance of 5.5×10^{-4} W/cm^2 at 4.5 cm). The gas ratio was controlled by adjusting the individual mass flow of each gas (total gas flow rate was 376 ml/min). H_2O_2 was added to the reactor as a photoinitiator at a rate of 1 mL/h using a syringe pump. Treatment duration was set to 1h. A valve was placed at the reactor outlet to control the operating pressure in the reactor, maintained at 10 kPag for all experiments (Dion et al. 2014). When the experiments were completed, the copper sample holders were carefully taken out of the reactor for analysis. All the surface treatments were carried out *in triplicata*.
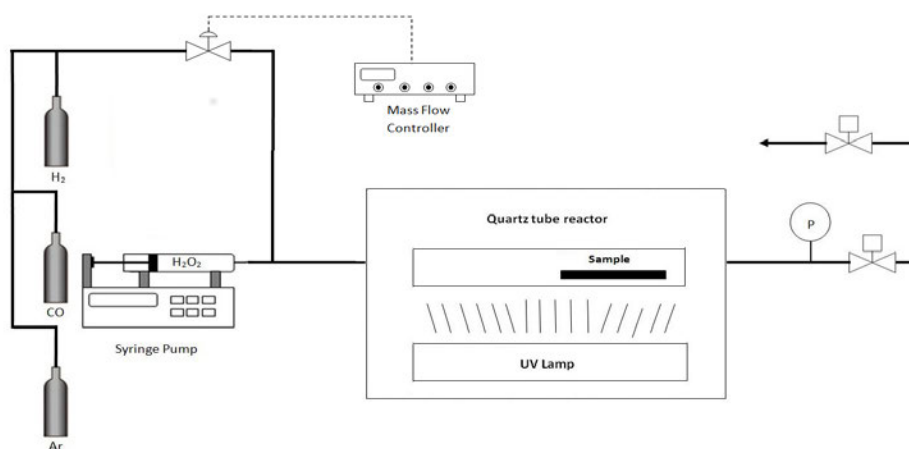

Fig. 1 Schematic of the PICVD reactor

Contact angle measurements. 50 µL of the untreated SPIONs suspension were deposited onto polished copper sample holders three successive times and allowed to dry at room temperature for 24 hours. The treated SPIONs were taken directly from PICVD. The contact angle measurements were achieved by placing 2 µL of deionized water on the samples. The sessile drop contact angle being stable on the minute time frame, one measurement per location was taken immediately using a FDS contact angle system OCA DataPhysics TBU 90E. The measurements were carried out on several spots on the untreated and treated SPIONs. In order to prepare the dispersion of SPIONs at a concentration of 12 mg/mL in water, sonication over 5 minutes with a Cole Parmer 500 watt ultrasonic homogenizer (CP505) was conducted.

Fourier Transform Infrared (FTIR) Spectroscopy. Using a Perkin Elmer spectrum 65 FTIR spectrometer, attenuated total absorbance probe, in the range of 600-4000 cm^{-1}, FTIR spectra at 4 cm^{-1} resolution were recorded. 32 scans were collected to improve the signal-to-noise ratio.

Transmission Electron Microscopy. A high-resolution transmission electron microscope (HRTEM) JOEL JEM 2100F was used for imaging the SPIONs. Analysis of the TEM images was carried out with the Gatan Digital Micrograph software. Average sizes of the untreated and treated SPIONs were calculated on the basis of 50 nanoparticles for each sample.

X-Ray Photoelectron Spectroscopy. Survey and C1s, O1s, and N1s high resolution spectra of SPIONs were obtained on a VG ESCALab 3 Mk II, using nonmonochromated Mg Kα radiation (1253.6 eV), at a power setting of 300 W, having an instrument resolution of 0.7 eV. The samples were deposited onto silica substrates, using two-sided adhesive Cu tape. The base pressure during scanning was less than 1×10^{-9} torr. Electrons were detected at a perpendicular take-off angle, using 0.05 eV steps, and spectra were analyzed using the VG Avantage software.

Results and discussion

Contact angle measurement. Figure 2 shows the results of the contact angle measurement of the bare, positively and negatively charged SPIONs before and after surface treatment with PICVD.
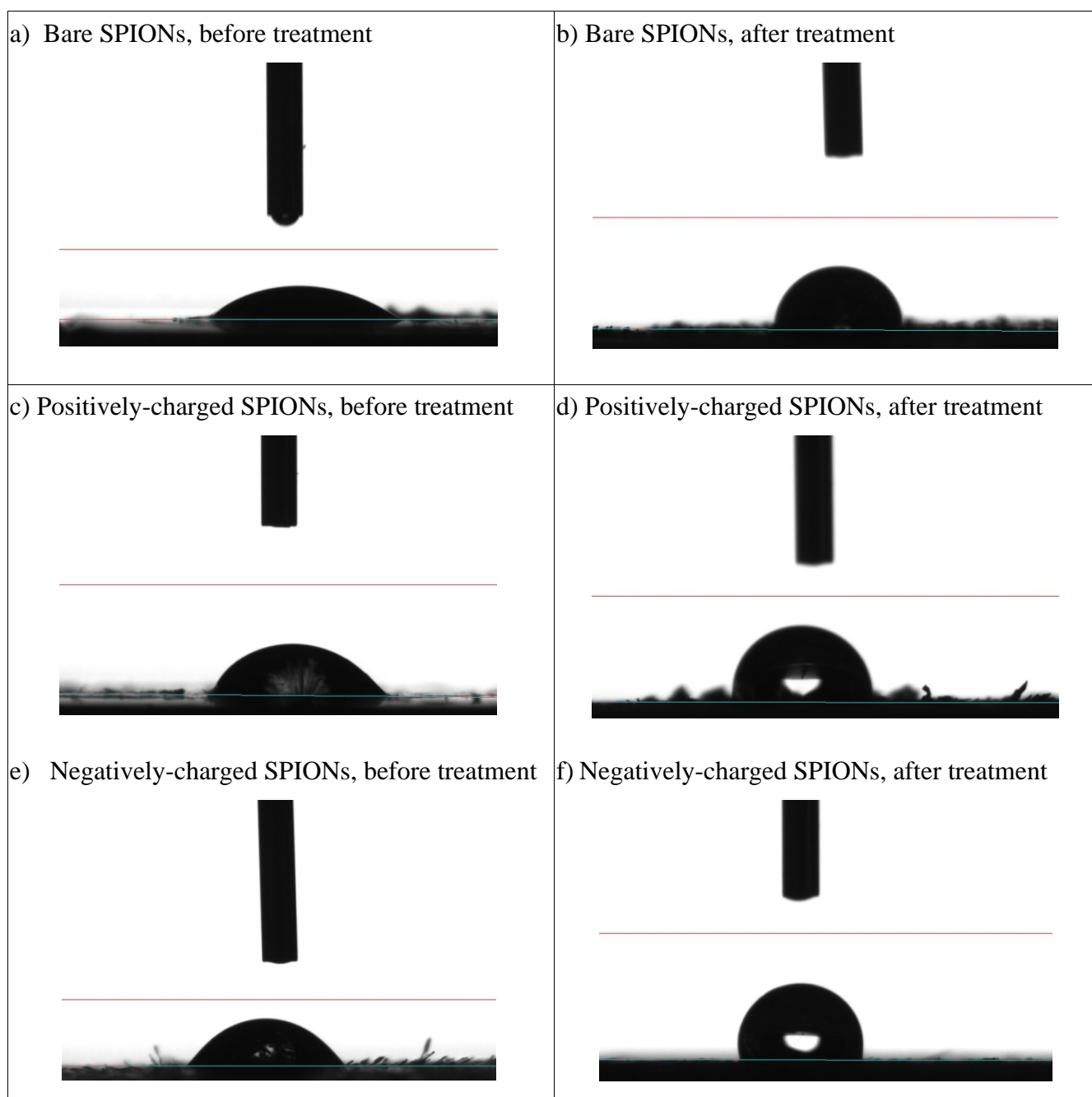
Fig. 2: Contact angle of (a,b) bare, (c,d) positively charged and (e,f) negatively charged SPIONs before and after surface treatment with PICVD, respectively

The average values of the contact angle of the untreated and treated bare, positively and negatively charged SPIONs are reported in Table 1. Essentially, these results demonstrate that the initial surface

charge plays no role in the final behaviour of the SPIONs, from a wettability perspective Ð both positively and negatively-charged SPIONS take on a hydrophobic behaviour post-treatment, as expected by the treatment conditions retained (Dion et al. 2014). Figure 3 shows treated SPION samples dispersed in water Ð these exhibit sedimentation, likely as a result of increased hydrophobicity (visual inspection).

Table 1: The average values of the contact angles of the untreated and treated bare, positively- and negatively-charged SPIONs

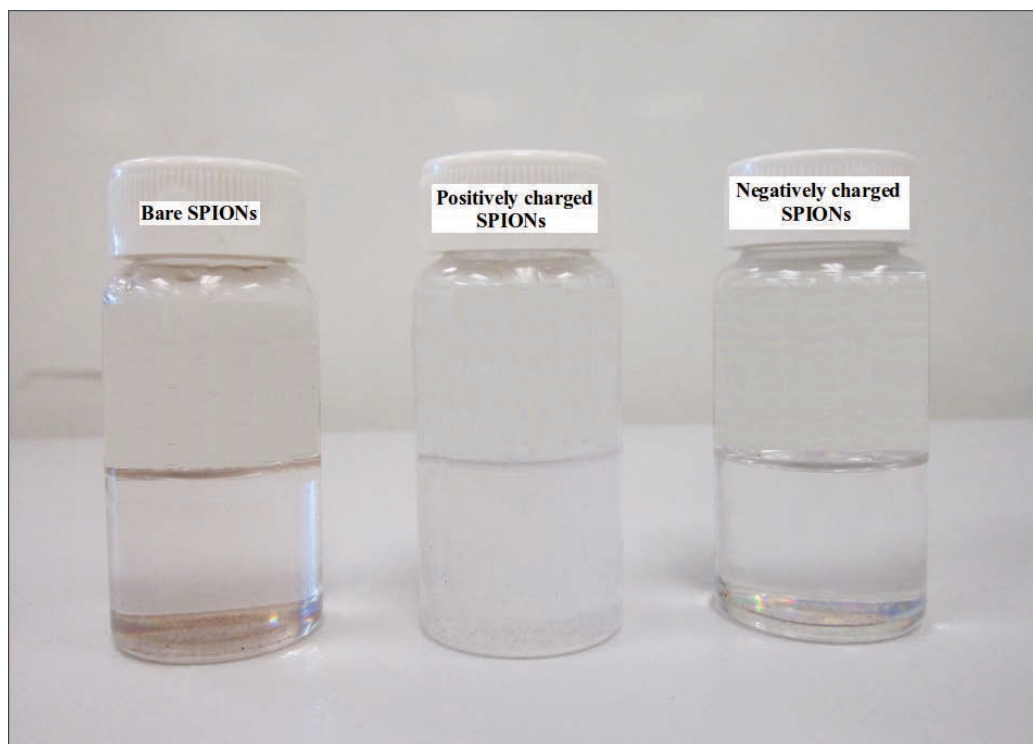| Samples!	Untreated!	Treated!
Bare SPIONs!	40¡ ± 9¡!	77¡ ± 14¡
Positively-charged SPIONs!	58¡ ± 12¡!	100¡ ± 23¡!
Negatively-charged SPIONS!	47¡ ± 13¡!	97¡ ± 15¡!

Fig. 3: Bare and treated SPIONs suspended in water

FTIR analysis of the SPIONs. Figure 4a, 4c and 4e show the FTIR spectra of the bare, positively and negatively charged untreated SPIONs, respectively. The peaks at 635 cm^{-1}, 1000 cm^{-1} (highlighted in Figure 4a) and the strong band at 1330 cm^{-1} are attributed to the Fe-O and the C-O bonds of the CH$_2$-OH groups, respectively. The peak that appears at 1690 cm^{-1} in the FTIR spectra of positively charged SPIONs corresponds to the amine bending mode (Kazemzadeh et al. 2012; Stuart 2004). The Si-O vibrational bond, which is due to the silica shell on the surface of positively and negatively charged SPIONs, appears at around 1100 cm^{-1} (Misra et al. 2003). The broad band at 3400Ð3500 cm^{-1} corresponds to the presence of surface hydroxyl groups.!The vibrations at around 1555 cm^{-1} and 1420 cm^{-1} are attributed to asymmetric and symmetric stretching of COO$^-$ group (Namanga et al. 2013). Figures 4b, 4d and 4f show the FTIR spectra of the bare, positively and negatively charged treated SPIONs, respectively. In these spectra, the peak at 1650 cm^{-1} is attributed to the C=C alkenyl stretching, which is absent in those of the untreated SPIONs. The peak at 880 cm$^-$1, which is attributed to =C-H bending, is absent in the spectrum of the untreated negatively charged SPIONS, but appears in that of the treated sample. These last two peaks are attributed to the polymer-like coating on the treated nanoparticles.
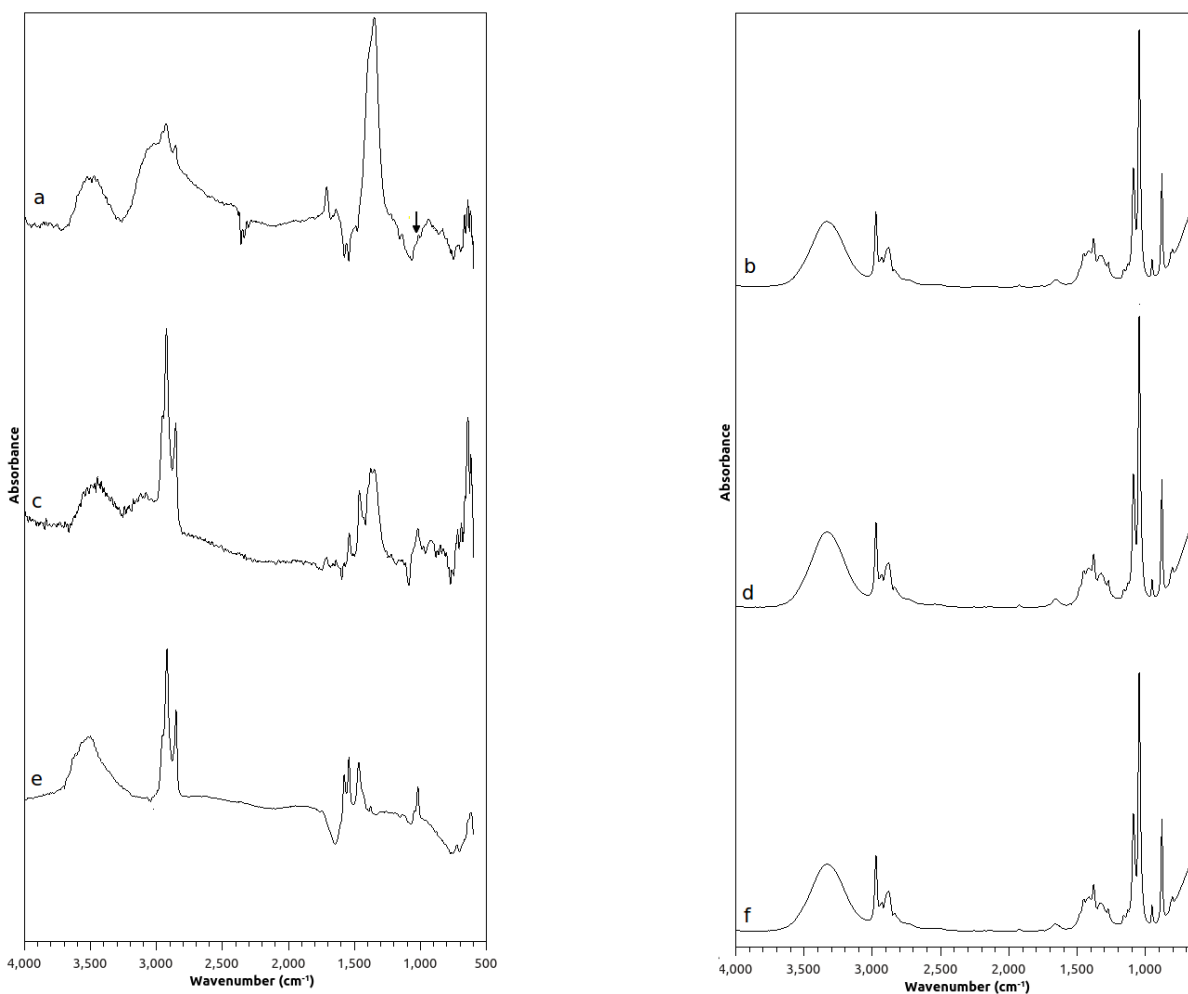
Fig. 4: FTIR spectra of a) bare, c) positively charged and e) negatively charged untreated SPIONs, b) bare, d) positively and f) negatively charged treated SPIONs

Transmission Electron Microscopy. Figure 5 shows the morphology of the untreated and treated SPIONs through TEM. The additional shell on their surface corresponds to the polymer coating imparted by the PICVD treatment. The average size distributions of untreated and treated SPIONs were calculated on the basis of fifty nanoparticles selected randomly in each sample type (Table 2). It should be noted that the values presented in Table 2 included both coated and uncoated particles (treatment efficiency is not 100%, especially in the case of the positively-charged SPIONs). This artificially creates an overlap between the coated and uncoated data Ð the user is referred to Figure 5 to clearly observe the presence of the coating. The increase in the average size of the charged SPIONs in comparison to the bare SPIONs confirms the surface functionalization of the samples due to the

presence of the silica shell on their surface. The average size of negatively charged treated SPIONs was more than that of the positively charged treated SPIONs. This indicates a thicker layer of polymers on the surface of the negatively charged treated SPIONs in comparison to the positively charged treated SPIONs. The average width of the polymers on the treated SPIONs was 1.5 nm. Moreover, the polymer coating deposited on the surface of the charged SPIONs seems to have affected their surface charge and caused aggregation.. The polymer appears heterogeneous, likely a result of the reactor geometry used.

X-ray Photoelectron Spectroscopy. The peaks of carbon, oxygen, nitrogen and iron were observed in the survey spectra of the untreated and treated SPIONs (data not shown). A small peak of silicon, corresponding to the substrate, was also observed. The high-resolution O1s spectra of the untreated and treated bare, positively- and negatively-charged SPIONs are shown in Figure 6. In Figure 6a, the peak at 533 eV is attributed to an oxygen atom in a O-C bond (Johansson and Campbell 2004). The peaks at 532 eV and 531 eV are attributed to C=O and COOH bonds, respectively. The peak at 528.5 eV is attributed to O-Fe bond. The same peaks are observed in Figures 6b, 6c and 6d. In Figure 6e, the peaks at 533 eV, 531.7 eV, 530 eV and 529.5 eV are attributed to O-C, C=O, COOH and O-Fe bonds, respectively. In Figure 6f, the peaks at 533 eV, 532 eV, 530.5 eV and 529.5 eV are attributed to O-C, C=O, COOH and O-Fe bonds, respectively. The O/C ratio of the bare SPIONs increased after treatment (Table 3). For negatively-charged SPIONs, this ratio decreased after PICVD surface modification. The O/C ratio of the positively-charged SPIONs was unaffected by treatment. This may be due to the same quantity of C and O of the coating on the surface of these nanoparticles. Indeed, this is supported by the fact that we observe a change in the wettability of these samples, as well as a coating via TEM. We hypothesize that negatively-charged electron cloud of the oxygen atoms imposed restrictions on the positioning of oxygen atoms on the surface of negatively-charged SPIONs (repulsive electrostatic interaction).
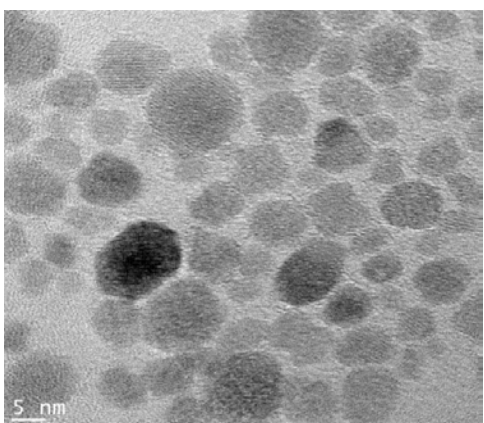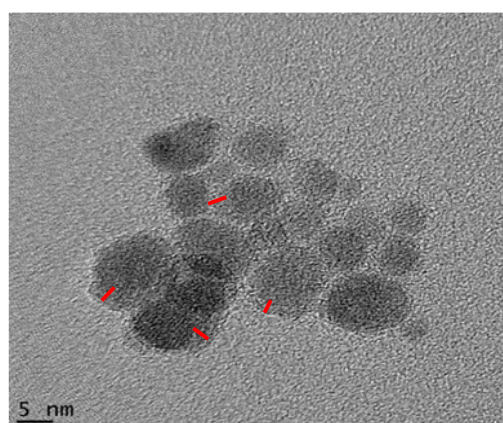
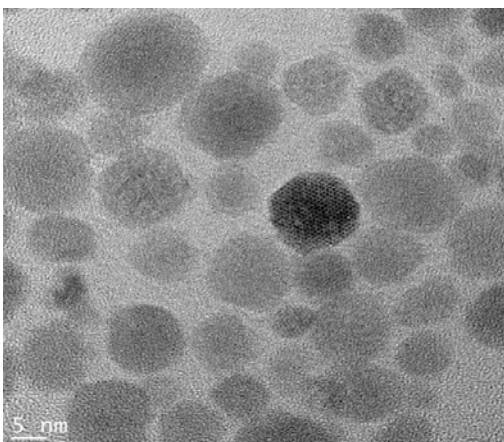a) Bare SPIONs, before treatment
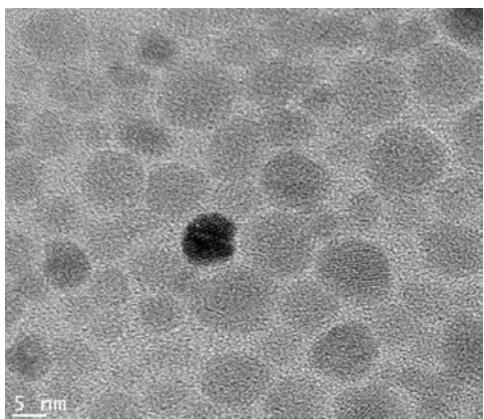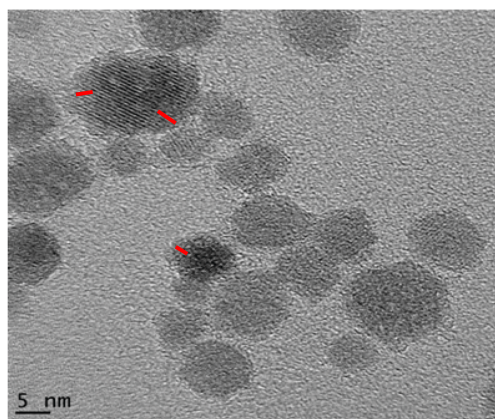
b) Bare SPIONs, after treatment

c) Positively-charged SPIONs, before treatment!

d) Positively-charged SPIONs, after treatment

e) Negatively charged SPIONs before treatment
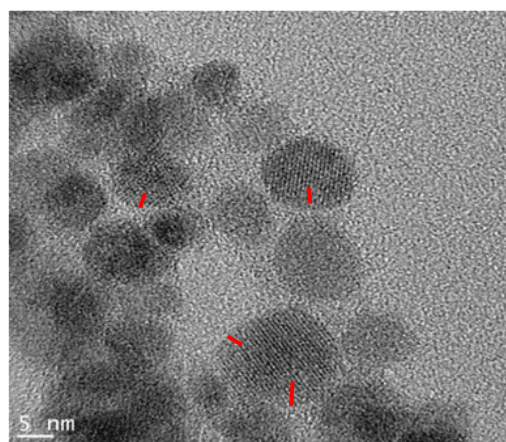
f) Negatively-charged SPIONs, after treatment

Fig. 5 TEM images of untreated and treated (a,b) bare, (c,d) positively charged and (e,f) negatively charged treated SPIONs. The crystalline shape of SPIONs and the amorphous shape of their polymer-coating (highlighted in red) are seen at 5 nm scale

Table 2 Average size distribution of untreated and treated SPIONs

Sample	Untreated [nm]	Treated [nm]
Bare SPIONs	10.9 ± 0.2	12.5 ± 0.4
Positively-charged SPIONs	11.8 ± 0.3	12.3 ± 0.3
Negatively-charged SPIONs	12.2 ± 0.2	13.6 ± 0.2

Table 3 Data on the O/C percentage ratios of untreated and treated SPIONs

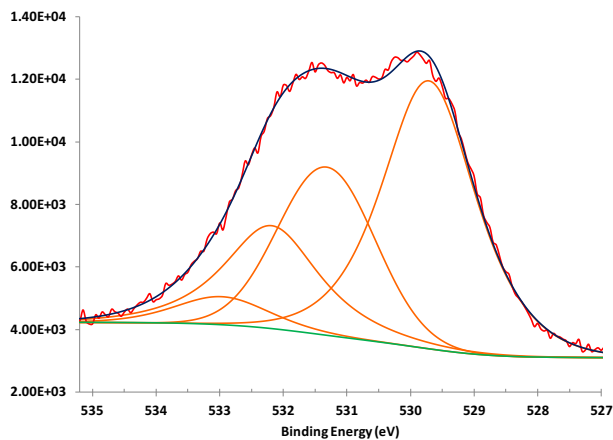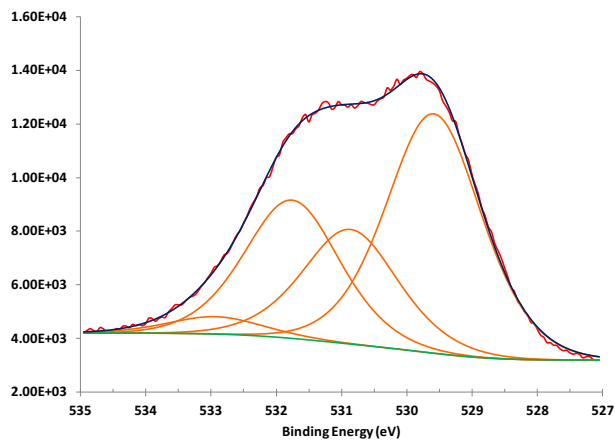| Samples	Untreated	Treated
Bare SPIONs	1.7	1.9
Positively-charged SPIONs	1.7	1.7
Negatively-charged SPIONs	1.7	0.7

a) Bare SPIONs, before treatment
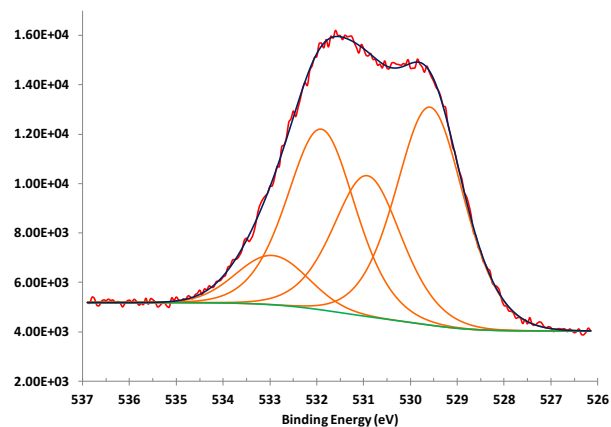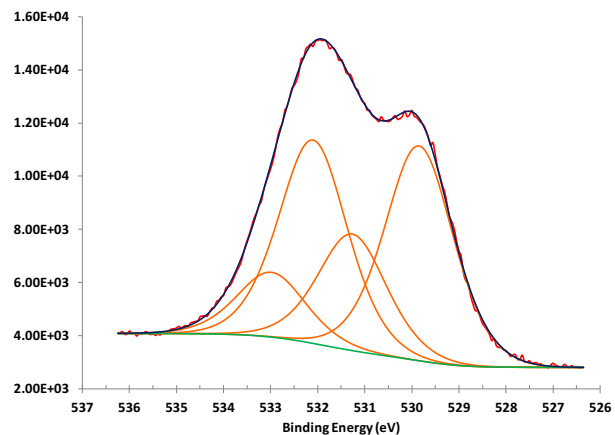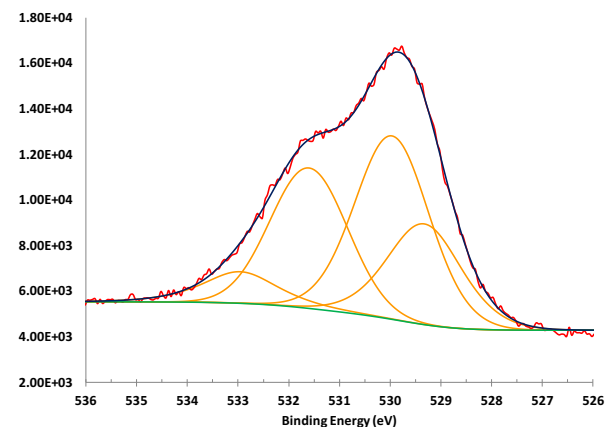
b) Bare SPIONs, after treatment

c) Positively-charged SPIONs, before treatment

d) Positively-charged SPIONs, after treatment

e) Negatively-charged SPIONs, before treatment
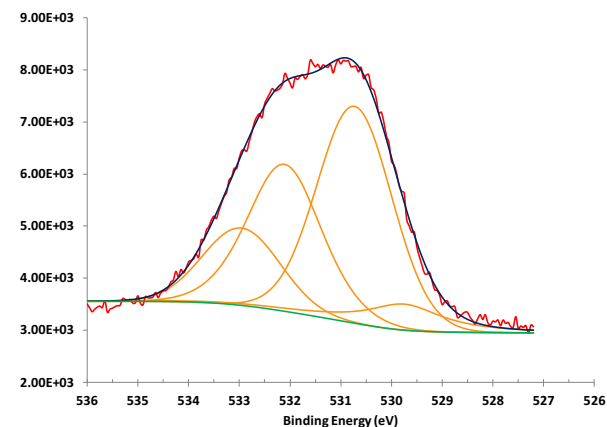
f) Negatively-charged SPIONs, after treatment

Fig. 6 XPS O1s high resolution spectra of a,b) bare, c,d) positively and e,f) negatively charged untreated and treated SPIONs

In this study, contact angle measurements, TEM and FTIR analyses of treated and untreated SPIONs confirm the presence of a polymer coating resulting from functionalization with PICVD. The photochemical reaction in PICVD can create large molecules of the form $C_xH_yO_z$, as well as water. As reported by (Dion et al. 2014), the coating has a structure similar to that of phenol formaldehyde, though this is strictly an approximation of the make-up of the highly cross-linked, polymer-like film.

The wettability on the surface of the treated SPIONs shows the change of their surface polarity. The XPS analysis shows that the surface chemical composition of the treated SPIONs is different depending on the initial surface charge. The difference of the O/C ratios of the untreated and treated bare, positively charged and negatively charged SPIONs in their high resolution XPS spectra leads to the suggestion that surface functionalization of these nanoparticles were carried out differently depending on their surface neutrality or charge. Although wettability does not seem to be affected, the data indicates more oxygen on the surface of the bare SPIONs compared to carbon (as expect), whereas there was no preference for these atoms on the surface of the treated positively charged SPIONs and the inverse tendency, which is the increase in the O/C ratio, was observed for the treated negatively charged SPIONs. The bare SPIONs with no surface charge showed a better spatial arrangement of oxygen than carbon atoms due to available sites for the positioning of these atoms on their surface after surface treatment. The site availability of the bare SPIONs is due to the absence of functional groups on their surface during their synthesis before their surface treatment with PICVD. Therefore, both the surface charge and stereochemical may have effects on the polymeric coating of SPIONS with this technique. An extensive investigation is needed to determine these effects in the coating of these nanoparticles and their dispersibility in micelle-forming molecules, as well as the applications of these nanoparticles for magnetic data storage, polluting agent removal and catalysis of organic reactions. For example, in the case of biomedical applications, nanoparticle agglomeration can cause significant toxic effects, namely through accumulation in the spleen and liver. The agglomeration of nanoparticles is possible after their surface treatment. In this study, we focused specifically on the surface chemistry of SPIONs, but further investigations are needed to determine the impact of surface treatment by PICVD on nanoparticle agglomeration.

Conclusion

Bare, positively and negatively charged SPIONs were treated by PICVD and their physicochemical properties due to their charge effect were determined. The significant increase in their contact angle with water indicated that their treatment with this technique made their surface non-polar. TEM and FTIR analyses showed the presence of nanometric polymeric coating around the SPIONs attributable to PICVD surface modification. XPS analysis of untreated and treated SPIONs revealed the surface charge effect on the polymeric coating of the samples, affecting the resulting O/C ratio. The data presented here will be a versatile resource for further surface studies of these nanoparticles. The control of the ratio of functional groups on the surface of treated SPIONs can lead to the preparation of mixed-monolayer nanoparticles for future experiments. Further investigation on the duration of the surface treatment of SPIONs with PICVD, coupled with modifying the core-size of the SPIONs before treatment, are warranted to assess the impact on the stability of the treated nanoparticles in different solvents (and therefore as an indication of performance in the intended applications).

References

Bloemen M, Stappen TV, willot P et al. (2014) Heterobifunctional PEG ligands for bioconjugation reactions on iron oxide nanoparticles. Plos One 9 e109475

Chang SY, Zheng N-Y, Chen C-S, Chen C-D, Chen Y-Y, Wang CRC (2007) Analysis of peptides and proteins affinity-bound to iron oxide nanoparticles by MALDI MS.!J Am Soc Mass Spectr 18:910Ð918

Chen CL, Zhang H, Ye Q, Hsieh WY, Hitchens TK, Shen HH, Liu L, Wu YJ, Foley LM, Wang SJ, Ho

C (2011) A new nano-sized iron oxide particle with high sensitivity for cellular magnetic resonance imaging. Mol Imaging Biol 13:825Ð839

Chen FF, Gerion D, Gray JW, Budinger TF (2009) Multimodal imaging probes for in vivo targeted and non-targeted imaging and therapeutics. US Patent WO2009045579 A2

Das M, Mishra D, Maiti TK, Basak A, Pramanik P (2008) Bio-functionalization of magnetite nanoparticles using an aminophosphonic acid coupling agent: new, ultradispersed, iron-oxide folate nanoconjugates for cancer-specific targeting. Nanotechnol 19(41):415101

De Palma R, Peeters S, Van Bael MJ, Van den Rul H, Bonroy K, Laureyn W , Mullens J, Borghs G, Maes G (2007) Silane ligand exchange to make hydrophobic superparamagnetic nanoparticles water-dispersible. Chem Mater 19:1821Ð1831

Dion CAD, Raphael W, Tong E, Tavares JR (2014) Photo-initiated chemical vapor deposition of thin films using syngas for the functionalization of surfaces at room temperature and near-atmospheric pressure. Surface Coat Technol 244:98Ð108

Eigler DM, Heinrich AJ, Loth S, Lutz CP: Antiferromagnetic storage device. United States Patent Patent N¡ US8,724,376 B2. 2014

Fan C, Gao W, Chen Z, Fan H, Li M, Deng F, Chen Z (2011) Tumor selectivity of stealth multi-functionalized superparamagnetic iron oxide nanoparticles. Int J Pharm 404:180Ð190

Gawande MB, Branco PS, Varma RS (2013) Nano-magnetite (Fe_3O_4) as a support for recyclable catalysts in the development of sustainable methodologies. Chem. Soc. Rev. 42:3371Ð3393

Georgelin T, Moreau B, Bar N, Villemin D, Cabuil V, Horner O (2008) Functionalization of Fe_2O_3 nanoparticles through the grafting of an organophosphorous ligand. Sens Actuat B Chem 134:451Ð454

Hanini A, Schmitt A, Kacem K, Chau F, Ammar S, Gavard J (2011) Evaluation of iron oxide nanoparticle biocompatibility" Int J Nanomed 6:787Ð794

Hu X, Yu JC, Gong J (2007) Fast production of self-assembled hierarchical αÐFe_2O_3 nanoarchitectures. J Phys Chem C 111: 11180Ð11185

Jin H, Hong B, Kakar SS, Kang KA (2008) Tumor-specific nano-entities for optical detection and hyperthermic treatment of breast cancer. Adv Exp Med Biol 614:275Ð284

Johansson L-S, Campbell JM (2004) Reproducible XPS on biopolymers: cellulose studies. Surface

Interf Analysis 36:1018−1022

Kazemzadeh H, Ataei A, Rashchi F (2012) Synthesis of magnetite nanoparticles by reverse co-precipitation. International J Modern Phys: Conference Series 5:160Ð167

Misra D, Wšrhoff K, Mascher P (2003) Dielectrics in Emerging Technologies: Proceedings of the International Symposium. Electrochem Soc Proc

Namvari M, Namazi H (2014) Clicking graphene oxide and Fe3O4 nanoparticles together: an efficient adsorbent to remove dyes from aqueous solutions. Int J Environ Sci Technol 11:1527Ð1536

Neouze MA, Schubert U (2008) Surface modification and functionalization of metal and metal oxide nanoparticles by organic ligands. Monatsh Chem 139:183−195

Nethaji S, Sivasamy A, Mandal AB (2013) Preparation and characterization of corn cob activated carbon coated with nano-sized magnetite particles for the removal of Cr(VI). Bioresour. Technol. 134:94Ð100

Obermayer D, Balu AM, Romero AA, Goessler W, Luque R, Kappe CO 2013) Nanocatalysis in continuous flow: supported iron oxide nanoparticles for the heterogeneous aerobic oxidation of benzyl alcohol**.** Green Chem*.* 15:1530-1537

Robinson I, Tung LD, Maenosono S, WŠlti C, Thanh NTK (2010) Synthesis of core-shell gold coated magnetic nanoparticles and their interaction with thiolated DNA*.* Nanoscale 2:2624-2630

Solans C, Izquierdo P, Nolla J, Azemar N, Garcia-Celma MJ (2005) Nano-emulsions. Curr Opin Colloid Interface Sci 10:102Ð110

Stanicki D, Boutry S, Laurent S, Wacheul L, Nicolas E, Crombez D, Elst LV, Lafontaine DLJ, Muller RN (2014) Carboxy-silane coated iron oxide nanoparticles: a convenient platform for cellular and small animal imaging. J Mater Chem B 2(4):387-397

Stuart BH (2004) Infrared spectroscopy: fundamentals and applications. Wiley Press

Sun S, Zeng H (2002) Size-Controlled Synthesis of Magnetite Nanoparticles. J Am Chem Soc 124:8204Ð8205

Uzun K, , evik O, Şenel M, Sšzeri H, Baykal A, Abasiyani MF, Toprak MS (2010) Covalent immobilization of invertase on PAMAM-dendrimer modified superparamagnetic iron oxide nanoparticles. J Nanopart Res 12:3057Ð3067

Veiseh O, Gunn J, Zhang M (2010) Design and fabrication of magnetic nanoparticles for targeted drug delivery and imaging. Adv Drug Deliv Rev 62(3):284Ð304

Vijayakumar R, Koltypin Y, Felner I, Gedanken A (2000) Sonochemical synthesis and characterization of pure nanometer-sized Fe_3O_4 particles. Mater Sci Eng A 286:101Ð105

Wang X, Liu L-H, Ramstršm O, Yan M (2009) Engineering nanomaterial surfaces for biomedical applications. Exp Biol Med 234:1128−1139

Wu W, He Q, Jiang C (2008) Magnetic Iron Oxide Nanoparticles: Synthesis and surface functionalization strategies. Nanoscale Res Lett 3:397Ð341